Effect of SiO_2 on Relaxation Phenomena and Mechanism of Ion Conductivity of [Nafion/$(SiO_2)_x$] Composite Membranes†

Vito Di Noto,*,‡ Rocco Gliubizzi,‡ Enrico Negro,‡ and Giuseppe Pace§

Dipartimento di Scienze Chimiche, Università di Padova, Via Marzolo 1, 35131 Padova (Pd), Italy, and Istituto di Scienze e Tecnologie Molecolari, ISTM-CNR c/o Dipartimento di Processi Chimici dell'Ingegneria, Via Marzolo 9, 35131 Padova (Pd), Italy

Received: August 4, 2006; In Final Form: October 5, 2006

This report describes a study of the effect of SiO_2 nanopowders on the mechanism of ionic motion and interactions taking place in hybrid inorganic−organic membranes based on Nafion. Five nanocomposite membranes of the formula [Nafion/$(SiO_2)_x$] with SiO_2 ranging from 0 to 15 wt % were prepared by a solvent casting procedure. TG measurements demonstrated that the membranes are thermally stable up to 170 °C but with the loss water it changes the cluster environments and changes the conductivity properties. MDSC investigations in the 90−300 °C temperature range revealed the presence of three intense overlapping endothermal peaks indicated as I, II, and III. Peak I measures the order−disorder molecular rearrangement in hydrophilic polar clusters, II corresponds to the endothermic decomposition of $-SO_3$ groups, and III describes the melting process in microcrystalline regions of hydrophobic fluorocarbon domains of the Nafion moiety. ESEM with EDAX measurements revealed that the membranes are homogeneous materials with smooth surfaces. DMA studies allowed us to measure two relaxation modes. The mechanical relaxation detected at ca. 100 °C is attributed to the motion of cluster aggregates of side chains and is diagnostic for $R-SO_3H\cdots SiO_2$ nanocluster interactions. DMA disclosed that at $SiO_2/^-SO_3H$ (ψ) molar ratios lower than 1.9, the oxoclusters act to restrict chain mobility of hydrophobic domains of Nafion and the dynamics inside polar cages of [Nafion/$(SiO_2)_x$] systems; at ψ higher than 1.9, the oxoclusters reduce the cohesiveness of hydrophilic polar domains owing to a reduction in the density of cross-links. FT−IR and FT−Raman studies of the [Nafion/$(SiO_2)_x$] membranes indicated that the fluorocarbon chains of Nafion hydrophobic domains assume the typical helical conformation structure with a $D(14\pi/15)$ symmetry. These analyses revealed four different species of water domains embedded inside polar cages and their interconnecting channels: (a) bulk water [$(H_2O)_n$]; (b) water solvating the oxonium ions directly interacting with sulfonic acid groups [$H_3O^+\cdots SO_3^-$−]·$(H_2O)_n$; (c) water aggregates associated with H_3O^+ ions [$H_3O^+\cdot(H_2O)_n$]; and (d) low associated water species in dimer form [$(H_2O)_2$]. The conductivity mechanism and relaxation events were investigated by broadband dielectric spectroscopy (BDS). [Nafion/$(SiO_2)_x$] nanocomposite membranes were found to possess two different molecular relaxation phenomena which are associated with the α-relaxation mode of PTFE-like fluorocarbon domains and the β-relaxation mode of acid side groups of the Nafion component. Owing to their strong coupling, both these relaxation modes are diagnostic for the interactions between the polar groups of the Nafion host polymer and the $(SiO_2)_x$ oxoclusters and play a determining role in the conductivity mechanism of the membranes. The studies support the proposal that long-range proton charge transfer in [Nafion/$(SiO_2)_x$] composites takes place due to a mechanism involving exchange of the proton between the four water domains. This latter proton transfer occurs owing to a subsequent combination of domain intersections resulting from the water domain fluctuations induced by the molecular relaxation events of host Nafion polymer.

1. Introduction

Polymer electrolyte membrane fuel cells (PEMFCs) and direct methanol fuel cells (DMFCs) are the preferred sources of portable power because of their light weight and high power density.[1−5] Nowadays, investigation in this field is focused on one hand on improving the efficiency of electrode materials,[6−9] and on the other hand on increasing the performance of proton conducting materials.[10−14] Desirable properties of proton electrolyte membranes are the following: (a) chemical and electrochemical stability in the operating system; (b) mechanical strength and stability under operating conditions; (c) chemical properties of compounds that are compatible with the bonding requirements of membrane electrode assembly (MEA); (d) extremely low permeability to the reactant species; (e) high electrolyte transport, to maintain uniform electrolyte contact and prevent localized drying; (f) high proton conductivity to support high current densities with minimal resistive loss and zero electronic conductivity; and (g) low production cost compatible with application.[13−15]

Perfluorinated polymer electrolytes such as Nafion, Aciplex, Flemion, and Dow membranes are some of the most promising

* To whom correspondence should be addressed. E-mail: vito.dinoto@unipd.it.

† Presented at the 209th Meeting of the Electrochemical Society, Denver, Colorado, May 2006.

‡ Università di Padova.

§ Istituto di Scienze e Tecnologie Molecolari.

10.1021/jp0650331 CCC: $33.50 © 2006 American Chemical Society
Published on Web 11/21/2006

electrolyte membranes for polymer electrolyte fuel cells.[13] Nevertheless, the major drawbacks to their large-scale commercial use involve cost and low proton conductivities at temperatures higher than 100 °C and low humidity.[13,15,16] Over the past decade's efforts to overcome the drawbacks of perfluorinated polymer electrolytes, the following four classes of proton conducting materials have been proposed:[16−20] (a) partially fluorinated membranes; (b) composite membranes; (c) aromatic polymer membranes; and (d) hybrid inorganic−organic proton conducting membranes.[21,22] Organic−inorganic composite membranes consisting of Nafion modified by inorganic additives such as SiO_2, TiO_2, ZrO_2, zeolites, and zirconium phosphate have been proposed as promising electrolytes for application in fuel cells owing to the advantages of reduced methanol crossover and water retention properties at temperatures higher than 100 °C.[16−20] Nafion consists of a polytetrafluoroethylene backbone endowed with side chains terminated with a sulfonic acid group.[13] The literature contains many studies on the structure of Nafion polymers and their possible proton conducting mechanisms.[13] Two different groups of structural models have been proposed for Nafion polymers.[13] The first group includes models based on materials in which ionic clusters of 3−5 nm diameter are interconnected together in a three-dimensional structure through channels with a diameter of 1−1.5 nm. The acid-terminated side chains of the polytetrafluoroethylene backbone extend into the cages, giving rise to an inverted micelle structure in which water molecules are clustered. It was proposed that the average ionic cluster contains approximately 70 acid sites and 1000 water molecules, and that it is dispersed in a hydrophobic polytetrafluoroethylene medium with a cluster center-to-center periodicity ranging from 5 to 7 nm. The second group of models describe Nafion as a system in which fluorocarbon crystallites, ionic hydrophilic clusters, and amorphous hydrophobic regions of lower ionic water content coexist together and create irregularly shaped water aggregates with many interconnections.[13] Water embedded in bulk Nafion is of crucial importance for the modulation of membrane conductivity.[13,23−26] Detailed vibrational studies suggested that water molecules in bulk Nafion experience more or less three different interaction environments:[13,27−30] (a) bulk water; (b) acid water present in the vicinity of sulfonic ions forming ionic clusters; and (c) weakly hydrated H_3O^+ water. The literature includes several studies on the effect of SiO_2 filler on Nafion hybrid inorganic−organic proton conducting membranes.[19,31−35] Nevertheless, a satisfactory and well-grounded description of the properties and of the influence of SiO_2 on the conductivity mechanism of hybrid membranes is not yet available.

This report presents the results of studies directed exclusively at elucidating the effect of SiO_2 nanopowders on the structure, properties, and conductivity mechanism of [Nafion/$(SiO_2)_x$] nanocomposite membranes with $0 \leq x \leq 15$ wt %. This aim was pursued by studying six different films prepared by a solvent casting procedure at 80 °C from Nafion and SiO_2 dispersions.

The membranes were accurately characterized by means of thermal (TG and MDSC) and dynamic mechanical analyses (DMA), morphological measurements (ESEM), and vibrational (FT−IR, FT−Raman) and Broadband Dielectric Spectroscopy (BDS) measurements. Vibrational investigations (FT−IR and FT−Raman) were carried out to obtain information on the network structure and conformation of the Nafion host polymer and on the dipole−dipole, dipole−SiO_2, proton−dipole, and proton−SiO_2 interactions in bulk materials. Accurate thermoanalytical studies (TG and MDSC) were performed to investigate the effect of the SiO_2 concentration on the thermal stability of the membranes and the thermal transition events in the Nafion host polymer. The effect of the SiO_2 concentration on the thermomechanical stability of the composite materials was studied by DMA. The electrical response of the hybrid inorganic−organic membranes was investigated by BDS in the 40 Hz−10 MHz and 5−135 °C frequency and temperature range, respectively. The electrical spectra were analyzed in terms of real and imaginary components of permittivity ($\epsilon^*(\omega) = \epsilon'(\omega) - i\epsilon''(\omega)$) and conductivity ($\sigma^*(\omega) = \sigma'(\omega) + i\sigma''(\omega)$). Conductivity spectra were studied to accurately determine the σ_{DC} of the membranes as a function of temperature. Correlation of the results described yielded a plausible conductivity mechanism for the composite membranes and revealed the influence of the inorganic moiety on the intermolecular interactions between nanodomains composing the materials.

TABLE 1: Reagent Composition and Molar Ratios for [Nafion/$(SiO_2)_x$] Membranes.

reagents			molar ratios	
Nafion (g)	SiO_2 (g)	x (wt % of SiO_2)	ψ^a	φ^b (mequiv/g)
0.45		0	0	0.800
0.45	0.0169	3.76	0.79	0.787
0.45	0.0225	5	1.05	0.783
0.45	0.0405	9	1.90	0.771
0.45	0.0585	13	2.74	0.760
0.45	0.0675	15	3.16	0.754

[a] $\psi = \text{mol}_{SiO_2}/\text{mol}_{SO_3H}$. [b] $\varphi = \{(\text{mequiv}_{Nafion} + \text{mequiv}_{silica})\}/\{g_{composite}\}$.

2. Experimental Section

2.1. Reagents. A 5 wt % solution of Nafion ionomer with a proton exchange capacity of 0.8 mequiv/g (Alfa Aesar, ACS) was used as received. SiO_2 fumed with a diameter less than 70 nm and a proton exchange capacity of 0.45 mequiv/g (Aldrich, ACS grade) was further purified by standard methods. Solvents were supplied by Aldrich and further purified by standard methods. Bi-distilled/milli-Q water was used in all procedures.

2.2. Membrane Preparation. Five [Nafion/$(SiO_2)_x$] nanocomposite membranes with x ranging from 0 to 15 wt % were prepared by a general solvent casting procedure as follows. An appropriate amount of Nafion (ca. 0.45 g; see Table 1) in a water/alcohol solution was cast in a beaker and heated at 80 °C for 40 min to remove the low-boiling solvents. The brittle cast film thus obtained was dissolved in 7 mL of *N*,*N*-dimethylformamide (DMF) and mixed with the desired quantity of fumed SiO_2 (see Table 1). The resulting mixture was homogenized by treatment in a ultrasonic bath for 30 min. The obtained homogeneous solution was recast in a Petri dish at 80 °C for 2 h under a hot air stream. The resulting composite Nafion film was dislodged from the Petri dish with milli-Q water. The thickness of the prepared membranes ranged from 150 to 250 μm.

2.3. Membrane Activation. Membranes were activated and purified by the following four-step protocol. First, the composite film was heated at 80 °C in bi-distilled water for 1 h. It was then treated for 1 h with a 3 wt % solution of H_2O_2 at 80 °C and afterward soaked for 1 h in a solution of 1 M H_2SO_4 at 80 °C. Finally, the membrane was washed 3 times with bi-distilled water for 1 h at 80 °C. The prepared membranes were stored immersed in milli-Q water at room temperature.

2.4. Proton Exchange Capacity (PEC). The PEC of investigated materials was determined by titration of a heterogeneous solution with 2 mM NaOH. The heterogeneous solution

was prepared by suspending a suitable amount of SiO_2 powder or activated membrane in a 1 M KCl solution. To achieve a complete exchange of acid protons with potassium ions, the heterogeneous solution was allowed to equilibrate for 24 h before titration. To avoid carbonation of NaOH, the titration was carried out under inert nitrogen atmosphere. Table 1 reports parameters ψ and φ of the [Nafion/$(SiO_2)_x$] composite membranes. ψ is the molar ratio $SiO_2/^-SO_3H$ and φ corresponds to the total proton exchange capacity of membranes, which accounts for the PEC of Nafion and silica filler ($\varphi = (\text{mequiv}_{\text{Nafion}} + \text{mequiv}_{SiO_2})/g_{\text{composite}}$).

2.5. Instruments and Methods. The morphology of the investigated samples was examined by using a Philips XL30TMP environmental scanning electron microscope (ESEM) at an acceleration voltage of 20 kV and a pressure of 0.8 Torr. A vapor flow was used to eliminate the excess negative charge on the surface of the material produced by the microscope's electrons. Elemental X-ray fluorescent microanalyses were performed with an embedded EDAX system coupled with an energy-dispersive X-ray spectrometer equipped with a Si/Li detector.

Dynamic Mechanical Analyses (DMA) were carried out with a TA Instruments DMA Q800, using the film/fiber tension clamp. Temperature spectra were measured by subjecting a rectangular film sample of ca. 25 (height) × 6 (width) × 0.15 (thickness) mm^3 to an oscillatory sinusoidal tensile deformation at 1 Hz with an amplitude of 4 μm (0.05 N preload force). Measurements were carried out in the −10 to 200 °C temperature range at a rate of 4 deg/min. Before measurements the samples were dried for 24 h in air at 80 °C. The mechanical response data were analyzed in terms of the elastic (storage) modulus (E') and viscous (loss) modulus (E''). $\tan \delta = E''/E'$ was analyzed as a function of temperature to measure the material damping characteristics such as vibration and sound damping phenomena.

Thermogravimetric analysis was carried out with a high-resolution TGA 2950 (TA Instruments) thermobalance. A working N_2 flux of 100 cm^3/min was used. The TG profile was recorded in the $20 < T < 800$ °C temperature range, using open platinum pans loaded with ca. 7 mg of each sample. The heating rate was varied dynamically during the ramp in responce to the derivative of weight change from 50 to 0.001 deg/min. Sensitivity was set from 0.1 to 2%/min weight change. The balance resolution is 1 μg.

Modulated Differential Scanning Calorimetry (MDSC) measurements were carried out with a MDSC 2920 Differential Scanning Calorimeter (TA Instruments) equipped with the LNCA low-temperature attachment operating under a helium flux of 30 cm^3/min. Measurements were made with a heating rate of 3 deg/min in the $-50 < T < 350$ °C temperature range on ca. 7 mg of sample hermetically sealed in an aluminum pan.

FT−IR spectra in the medium infrared (MIR) region were obtained with a Nicolet FT−IR Nexus spectrometer equipped with a triglycine sulfate (TGS) detector at a resolution of 4 cm^{-1}. MIR measurements were derived by averaging 1000 scans obtained on samples dispersed in anhydrous KBr pellets. Baseline correction was performed with the Nicolet FT−IR Nexus spectrometer software.

Raman spectra were collected with a Nicolet FT−Raman module attached to a Nexus FTIR system. The spectra were collected at an angle of 90° with a spectral slit width of 4 cm^{-1}. The spectra were recorded at room temperature with samples sealed in Pyrex glass NMR tubes. The excitation line was 633 nm with a power of 0.52 W. Each spectrum was the result of the accumulation and averaging of 15 000 scans.

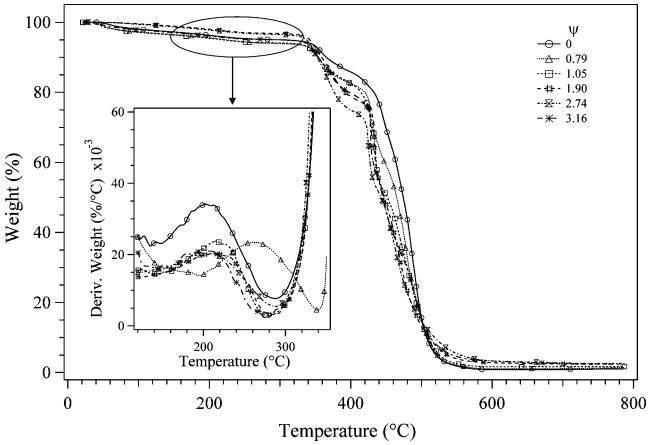

Figure 1. TG measurements of the [Nafion/$(SiO_2)_x$] membranes. The inset shows the dependence of the derivative of TG profiles on temperature.

Electrical spectra were measured in the 40 Hz−10 MHz frequency range, using an Agilent 4294A Impedance Analyzer. The temperature range from 5 to 135 °C was explored by using a Novocontrol Quatro cryostat operating with an N_2 gas jet heating and cooling system. As described in greater detail elsewhere,[36] the measurements were performed by sandwiching the samples between two circular platinum electrodes sealed within a CR2032 button battery case with a free volume of 0.30204 cm^3. The geometrical constant of the cell was obtained by measuring the electrode−electrolyte contact surface and distance between electrodes with a micrometer. No corrections for thermal expansion of the cell were carried out. The temperature was measured with an accuracy greater than ± 0.1 °C. The complex impedance ($Z^*(\omega)$) was converted into complex conductivity ($\sigma^* = \sigma' + i\sigma''$) and permittivity ($\epsilon^* = \epsilon' - i\epsilon''$) by using the following equations: $\sigma^* = k \cdot 1/Z^*(\omega)$ ($Z^*(\omega) = Z'(\omega) + iZ''(\omega)$) and $\sigma^* = i\omega\epsilon^*$ ($\sigma' = \omega\epsilon''$, $\sigma'' = \omega\epsilon'$), respectively, where k is the cell constant in cm^{-1} and $\omega = 2\pi f$ (f = frequency in Hz).

σ^* spectra were employed to investigate the AC electric response of the samples and to detect the corresponding bulk dc conductivity σ_{dc} as described elsewhere.[36]

3. Results and Discussion

3.1. Thermal Analyses and Morphology. The high-resolution TG curves shown in Figure 1 indicate that the [Nafion/$(SiO_2)_x$] composites are thermally stable up to ca. 170 °C. The first mass elimination, observed in the 80−150 °C temperature range, is attributed to the traces of water present in the composite materials. Accurate inspection of the derivative curve of high-resolution TG profiles, reported in the inset of Figure 1, indicates that a second mass loss is registered in the 170−250 °C temperature region, which, in agreement with other studies,[21] corresponds to the decomposition of $^-SO_3H$ groups. It should be noted that these observations are in contrast with other low-resolution TG studies which report that Nafion sulfonic groups decompose at temperatures higher than 280 °C.[10,13,37]

The decomposition process of $^-SO_3H$ groups in [Nafion/$(SiO_2)_x$] membranes is observed at temperatures slightly higher than that of Nafion 117 (ca. 189 °C). Indeed, as ψ increases (a) a better stability is reached in the region $0 < \psi \leq 1.90$ and (b) the decomposition temperature decreases to that of Nafion for $1.9 < \psi \leq 3.16$. These findings indicate that at $0 \leq \psi \leq 1.90$

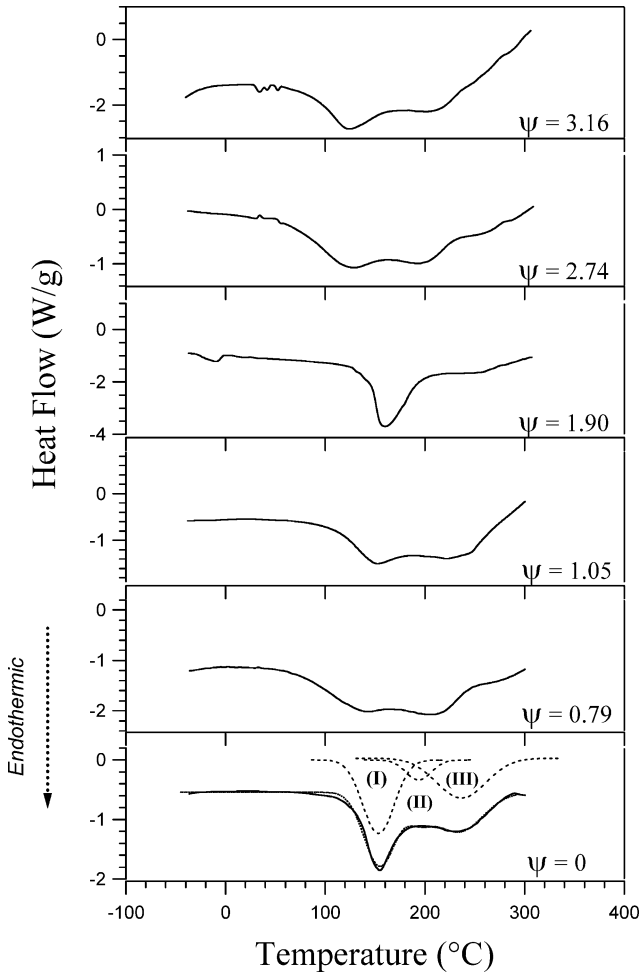

Figure 2. MDSC curves of the [Nafion/$(SiO_2)_x$] membranes with decomposition by Gaussian functions of the MDSC region in the 90−300 °C range. I, II, and III indicate the endothermic peaks that were detected.

the SiO_2-HSO_3-R interactions thermally stabilize the Nafion acid side groups. In this temperature region the [Nafion/$(SiO_2)_x$] composite underwent weight losses of ca. 2−3%, which correspond to a partial decomposition of sulfonic groups.

The weight loss observed in the 316−400 °C temperature region corresponds to the decomposition of Nafion polyether side chains.

In accordance with the literature,[37] the third mass elimination revealed in the 400−500 °C range is attributed to PTFE backbone decomposition. It should be observed that the inorganic moiety of [Nafion/$(SiO_2)_x$] systems reduces the thermal stability of both polyether side chains and PTFE backbone chains, thus indicating that no significant thermal stabilizing interactions occur between SiO_2 and the polymer host network.

The first MDSC scan (Figure 2) yielded three intense and overlapping endothermic peaks in the 90−300 °C temperature range. These transitions are indicated as I, II, and III and are peaking respectively in the lower, middle, and higher temperature wing of the described MDSC region (see peaks represented with dotted lines in Figure 2). The position of the endothermic peaks depends on the sample composition.

In particular, for pristine Nafion ($\psi = 0$), the onset temperatures for events I, II, and III are detected at ca. 122, 168, and 181 °C, respectively. I is assigned to the order−disorder molecular rearrangement transitions which occur due to the polymer relaxation process taking place inside Nafion's hydrophilic polar clusters. Indeed, it was demonstrated that this peak[37] is diagnostic for the anion−cation and acid side groups−water interactions of Nafion. Figure 2 and Table 2 show that in the region $0.79 < \psi \leq 1.9$, the onset temperature of I increases, while for $\psi > 1.9$ it decreases down to 63 °C. These observations can be explained if we assume that at $\psi \neq 1.9$ the $-SO_3H-SiO_2$ interactions become weaker, thus giving rise to polar clusters which are thermodynamically less stable than those present in pristine Nafion. In accordance with De Almeida et al.,[37] endothermic event III is attributed to the melting of hydrophobic fluorocarbon microcrystalline regions in the Nafion membranes. The event peaks at a point II corresponding to the temperature in the TG profiles at which a mass elimination associated with the decomposition of $^{-}SO_3H$ groups is measured (see inset in Figure 1). These findings prompt us to assign II to the endothermic decomposition of acid $^{-}SO_3H$ groups.

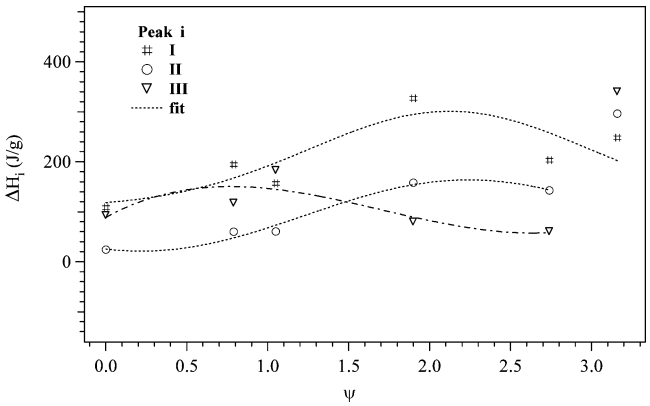

Figure 3. Dependence of ΔH_i (J/g) of i = I, II, and III endothermic peaks on ψ (see Table 1).

TABLE 2: MDSC Transition Temperatures (°C) of [Nafion/$(SiO_2)_x$] Membrane

	peak I		peak II		peak III	
ψ^a	onset	minimum	onset	minimum	onset	minimum
0	122	155	168	194	181	234
0.79	60	149	166	211	192	267
1.05	106	154	163	200	190	241
1.90	138	164	159	179	207	249
2.74	63	127	146	198	223	259
3.16	83	129	131	194	174	247

[a] $\psi = mol_{SiO_2}/mol_{\cdot SO_3H}$.

TG and MDSC results reveal that in the samples with $0.79 \leq \psi \leq 1.9$ the $^{-}SO_3H-SiO_2$ interactions act to thermally stabilize the polar clusters, the $^{-}SO_3H$ groups, and the hydrophobic PTFE backbone. These results were further supported by the ΔH values measured for events I, II, and III (Figure 3). ΔH values were evaluated as shown in Figure 2 by decomposition of MDSC curves with Gaussian functions. Figure 3 indicates that (a) ΔH_{III} is slightly affected by the SiO_2 oxocluster concentration and (b) ΔH_I and ΔH_{II} are dependent on SiO_2 in membranes and increase as ψ rises in the $0 < \psi \leq 1.9$ region.

Taken together, this detailed thermal analysis suggests that in the [Nafion/$(SiO_2)_x$] composites with $0.79 \leq \psi \leq 1.9$ the interaction between $^{-}SO_3H$ and SiO_2 oxoclusters gives rise to (a) a slight modulation of the enthalpy of the transition related to the PTFE backbone chains Nafion's hydrophobic domains, (b) an increase in the thermal stability of $^{-}SO_3H$ groups, and (c) an increase in the enthalpy of the thermal relaxation events occurring in hydrophilic-dipolar clusters of Nafion.

The morphology of the [Nafion/$(SiO_2)_x$] materials was investigated by SEM measurements. Selected micrographs of

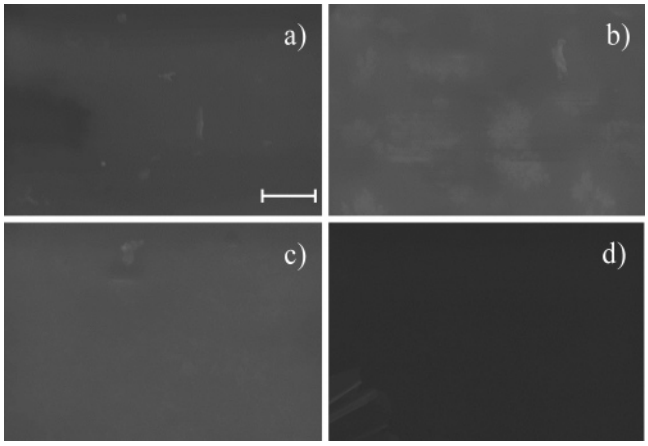

Figure 4. SEM micrographs of selected [Nafion/$(SiO_2)_x$] membranes: (a) $\psi = 0$; (b) $\psi = 0.79$; (c) $\psi = 1.90$; and (d) $\psi = 2.74$. The bar corresponds to a length of 5 μm.

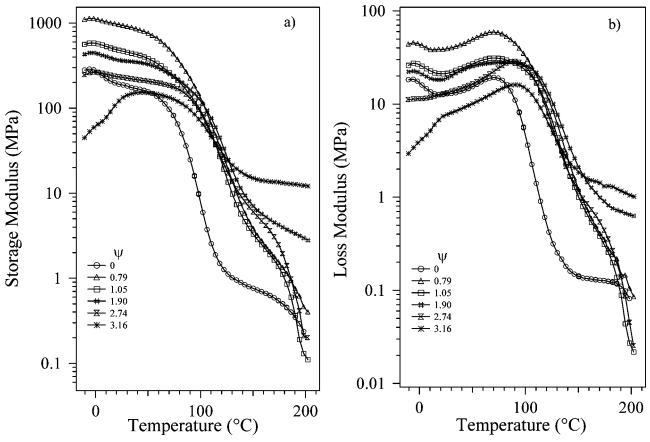

Figure 5. Analysis of [Nafion/$(SiO_2)_x$] membranes for temperature dependence of the storage modulus (E'; panel a) and loss modulus (E''; panel b).

[Nafion/$(SiO_2)_x$] membranes reported in Figure 4 demonstrate that the investigated systems present the typical appearance of a homogeneous gummy glassy material with a very smooth surface.

X-ray fluorescence analysis with energy dispersive spectroscopy (XRD-EDS) performed on different areas of the composite membrane surface indicated that C, O, Si, and S are uniformly distributed over the entire material. A careful analysis of backscattered images confirmed that the [Nafion/$(SiO_2)_x$] composites are very homogeneous materials, at least at this level of analysis.

3.2. Dynamic Mechanical Analysis. The effect of SiO_2 oxoclusters on the structural relaxation of the [Nafion/$(SiO_2)_x$] membranes was investigated by measuring the temperature spectra of tan δ, the loss modulus (E''), and the storage modulus (E'). These studies were performed by using a dynamic oscillatory method with small sinusoidal mechanical elongations (4 μm) at 1 Hz of frequency (see the Experimental Section). Plots of the logarithms of the storage and loss modulus on temperature recorded for Nafion (Figure 5) show a relaxation event at ca. 100 °C that on the basis of other studies of Nafion can be attributed to α-relaxation.[13,38] This mechanical relaxation mode was assigned to the motions in the cluster aggregates of side chains.[38] At temperatures above 170 °C an irreversible elongation of the sample in the instrument occurs. The peak revealed at ca. 19 °C in the E'' spectra corresponds to the β relaxation mode of Nafion and is assigned to the main chain

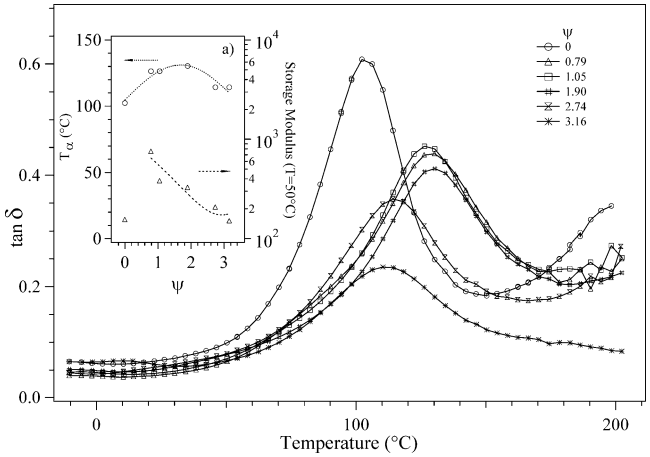

Figure 6. Tan δ versus T for [Nafion/$(SiO_2)_x$] membranes. The inset reports the dependence of the storage modulus on ψ, measured at 50 °C and 1 Hz. T_α is the temperature at the maximum of the tan δ peak.

motions in the fluorocarbon phase. It is possible to observe that the position of β relaxation seems to be slightly dependent on the SiO_2 concentration, probably owing to its very low intensity.

The profiles of E' vs temperature indicate that the membrane storage module value depends on the SiO_2 concentration in [Nafion/$(SiO_2)_x$] composites.

It is to be emphasized that (a) in the region $0.79 < \psi < 3.16$, E' measured at 50 °C (inset in Figure 6) decreases exponentially as ψ increases; (b) the E' value of the sample with $\psi = 3.16$ is coincident with that of Nafion reference material. If we consider that the number of interchain cross-links in a polymer network is proportional to the elastic modulus,[39,40] $E' = gnkT + E_{en}$, where k is Boltzmann's constant, T the thermodynamic temperature, E_{en} the contribution of polymer entanglements to E', g a constant value ranging from 0.6 to 1, and n the number density of interchain cross-links in a polymer network, two properties of the hydrophilic polar cages of nanocomposite become evident. First, the samples with the lowest ψ will have higher densities of dynamic interchain cross-links $R-SO_3H\cdots[SiO_2]\cdots HSO_3-R$ and thus higher values of E'. It should be highlighted that in [Nafion/$(SiO_2)_x$] with $\psi = 0.79$ each silica tetrahedron is interacting with ca. two acid $^-SO_3H$ terminated side groups. Second, as the SiO_2 concentration increases, the number of dynamic cross-links decreases thus reducing the E' modulus. Indeed, when $\psi = 3.16$ the storage modulus of [Nafion/$(SiO_2)_x$] systems corresponds to that of the pristine Nafion membrane, thus suggesting that the effect of dynamic cross-links on the mechanical properties of the materials is practically negligible.

Figure 6 reports tan δ on temperature. The dependence of the dynamic mechanical transition temperature, T_α, on ψ (Figure 6, inset) exhibits a parabolic curve with downward convexity and a maximum peaking at $\psi = 1.9$. Comparison of the temperature dependence of T_α with that of ΔH_I shown in Figure 3 suggests that these experimental observations are linked to the same physical phenomenon, which is modulated by the dynamics occurring within the polar cluster aggregates of the [Nafion/$(SiO_2)_x$] systems. On this basis it is easy to understand that for the membranes with ψ in the region $0 < \psi < 1.9$, owing to the presence of a higher density number of dynamic cross-links $R-SO_3H\cdots[SiO_2]\cdots HSO_3-R$, the thermal and mechanical stability of the polar cages is higher with respect to that of the materials having a different composition.

Taken together, the DMA analyses reveal that (a) the concentration of dynamic interacting cross-links existing be-

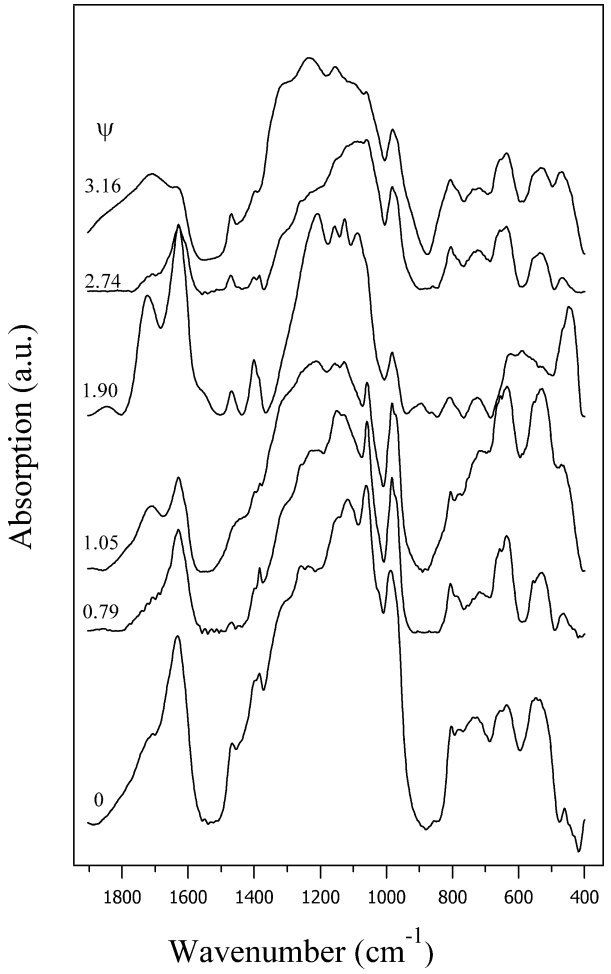

Figure 7. FT−IR absorption spectra of the [Nafion/$(SiO_2)_x$] membranes.

tween SiO_2 oxoclusters and HSO_3−R acid side groups of Nafion increases the mechanical stability of the membranes, thus demonstrating that the SiO_2 oxoclusters act to restrict both the main chain mobility of hydrophobic fluorocarbon domains and the mobility of polymer side chains inside polar cage aggregates (b) high SiO_2 concentrations ($\psi > 1.9$) reduce the cohesiveness of hydrophilic cage domains owing to a dilution of the density number of R−SO_3H···[SiO_2]···HSO_3−R cross-links.

3.3. FT−IR and FT−Raman Studies. The [Nafion/$(SiO_2)_x$] membranes were subjected to FT−IR and FT−Raman investigations to understand the structure and the interactions between the inorganic moieties and the Nafion macromolecular system.

The resulting MIR and FT−Raman spectra are reported in Figures 7 and 8. It should be noted that the FT−Raman spectrum of the membrane with $\psi = 3.16$ was impossible to measure owing to the strong fluorescence of the sample. These spectra present different features which are directly correlated with the vibrational modes of (a) the PTFE backbone component of hydrophobic domains of Nafion,[41−44] (b) the polyether side chains,[45,46] (c) the $^-SO_3H$ acid groups,[45,46] (d) the water species embedded in Nafion bulk composites,[27,47] and (e) the SiO_2 inorganic component.[48,49] The detected vibrational peaks are briefly summarized in Table 3 together with their correlative attributions.

The 400−1400 cm^{-1} region of the FT−IR and FT−Raman profiles present vibrational modes diagnostic for the PTFE backbone chain conformation. Table 3 reports the frequencies of Nafion PTFE domain vibrational modes together with their

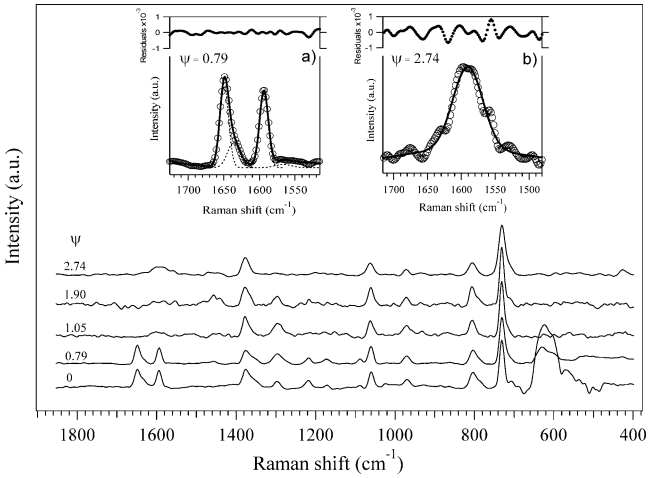

Figure 8. FT−Raman spectra of the [Nafion/$(SiO_2)_x$] membranes. The inset shows decomposition by Gaussion functions of the 1700−1500 cm^{-1} spectral region for selected samples.

symmetry class, which coincides with that of a fluorocarbon chain in a $D(14\pi/15)$ factor group.[41−44] It should be pointed out that as ψ increases, the narrow bands typical of crystalline PTFE spectra exhibit peak broadening owing to the crystallinity decrease in Nafion and in [Nafion/$(SiO_2)_x$] composites. This peak broadening seems to be similar to that of a PTFE sample with a crystallinity lower than 40%.[43,45] Furthermore, the location of fluorocarbon vibrations is unaffected by the SiO_2 concentration.

The bands peaking at 986 and 970 cm^{-1} are attributed to the ν_{as}(C−O−C) and ν_s(C−O−C) modes, respectively, of ether side chains.[45,46] It is to be noted that the profiles of these peaks are independent of the [Nafion/$(SiO_2)_x$] composition.

The bands measured at ca. 1059 cm^{-1} in the FT−IR and FT−Raman spectra are ascribed to the symmetric stretchings of $\nu_s(SO_3^-)$ acid groups.[45,46] In the FT−IR spectra this mode shows a peak intensity increasing as ψ decreases, thus suggesting that the coordination symmetry of R−SO_3H···[SiO_2]···HSO_3−R cross-linking sites in polar cages diminishes as ψ decreases. The FT−Raman spectra (Figure 8) confirm this observation by showing an increase in band broadening as ψ increases.

The strong peak in the FT−IR spectra at ca. 1207 cm^{-1} corresponds to the antisymmetric stretching mode of $\nu_{as}(CF_2)$ and $\nu_{as}(SO_3^-)$ groups. It is to be pointed out that the intensity of this peak is strongly influenced by the SiO_2 concentration in the [Nafion/$(SiO_2)_x$] materials.

The intensity peaking at 1088 cm^{-1} and associated with the $\nu(SiO_2)$ vibration strongly overlaps with the neighboring bands.[48,49]

The water bending vibrations in the 1590−1770 cm^{-1} range (Figure 9) are diagnostic vibrations for water species present in bulk Nafion and [Nafion/$(SiO_2)_x$] composite membranes.[27,47] Peak III, revealed in the FT−IR and FT−Raman spectra at ca. 1633 cm^{-1}, is ascribed to bulk water [$(H_2O)_n$] not associated with an H_3O^+ ion. The FT−IR spectral bands registered at 1722 and 1760 cm^{-1} are associated with the vibrations of hydrated oxonium ions $\delta([H_3O^+\cdots(H_2O)_n])$ (II) and with the hydrated oxonium ion clusters directly interacting with the R−SO_3^- anion, $\delta([H_3O^+\cdots SO_3^-]\cdot(H_2O)_n)$ (I), respectively. Semiquantitative information regarding the concentration of each type of water species was obtained by Gaussian decomposition of the spectrum in the 1600−1800 cm^{-1} region (Figure 9). This analysis permitted us to determine the peak position, the full width at half-maximum (fwhm), and the band areas. With

TABLE 3: FT−IR and FT−Raman Band Assignments of [Nafion/$(SiO_2)_x$] Composite Membranes

obsd freq (cm^{-1})[a]						
Nafion		composite membranes		band assignments[b]	symmetry class[c]	ref
FT−IR	FT−Raman	FT−IR	FT−Raman			
		465		r(Si−O)		48, 49
526 (m)		526 (m)		$\delta(CF_2)$	E_2	45
555 (m)		545 (m)	568 (w)	$t(CF_2)$	A_2	45
633 (m)	622 (vs,b)	638 (m)	622 (w, b)	$\omega,\delta(CF_2)$; (H_2O)	A_2	45
659 (sh, vw)						45
723 (w, b)	732 (vs)	717 (w, b)	732 (vs)	$\nu_s(CF_2)$	A_1	45
779 (vw, b)		779 (vw, b)			E_2	45
804 (w)	805 (m)	801 (w)	805 (m)	ν(C−S)		45
970 (sh)	969 (w)	970 (sh)	969 (w)	ν_s(C−O−C)		45, 46
987 (s)		986 (s)		ν_{as}(C−O−C)		45
1060 (vs)	1059 (m)	1062 (s)	1059 (m)	$\nu_s(SO_3^-)$		45, 46
		1088 (sh)	1089 (vw)	ν(Si−O)		48, 49
1160 (s)	1172 (vw)	1150 (s)	1172 (vw)	$\nu_{as}(CF_2)$	E_1	45
1207 (s)		1207 (s)		$\nu_{as}(CF_2)$, $\nu_{as}(SO_3^-)$	A_2	45, 46
1216 (sh)	1217 (w)	1221 (sh)	1217 (w)	$\nu_{as}(CF_2)$	E_1	45
1300 (sh)	1297 (w)	1302 (sh)	1297 (w)	ν(C−C)	E_2	45
1319 (sh)		1321 (sh)				45
1384 (m)	1377 (m)	1382 (m)	1377 (m)	ν_s(C−C)	A_1	45
1405 (sh)		1405 (m)		ν(S=O)		47
	1594 (m)		1594 (m)	$\delta([H_2O]_2)$		27
	1636 (sh)		1625 (sh)			27
1633 (w, b)	1649 (m)	1633 (w, b)	1649 (m)	$\delta([H_2O]_n)$		45
1722 (sh)		1722 (sh)		$\delta([H_3O^+(H_2O)_n])$		45
1760 (sh)		1760 (sh)		$\delta([H_3O^+-SO_3^-](H_2O)_n)$		27
2860 (w, b)		2863 (vw)		$\nu_3(H_3O^+)$	E	27, 47
3400 (s, b)	3300 (vs, b)	3400 (s, b)	3311 (vs, b)	$\nu_{hy}(H_2O)$		47

[a] Relative intensities of observed bands are reported in parentheses: vs, very strong; s, strong; m, medium; w, weak; vw, very weak; b, broad; sh, shoulder. [b] ν, stretching; δ, bending; ω, wagging; t, twisting; r, rocking; as, antisymmetric mode; s, symmetric mode. [c] $D(14\pi/15)$ symmetry class of the helical perfluorocarbon backbone.

respect to the total amount of water embedded in [Nafion/$(SiO_2)_x$] composite membranes, the percentage of each type of structurally different H_2O domain was determined by calculating f_i (%) $= A_i \cdot 100/\Sigma$, where A_i is the band area contributed by a defined type of water domains and $\Sigma = \sum_{i=1}^{3} A_i$. Figure 10 shows the dependence of f_i (%) on ψ for each type of water domain. It is possible to note that as ψ increases (a) the percentage of bulk water not associated with H_3O^+ increases linearly, (b) the concentration of hydrated oxonium ion clusters $[H_3O^+\cdots(H_2O)_n]$ decreases, and (c) the concentration of hydrated oxonium ions directly associated with sulfonic anion groups decreases. The dependence of f_I (%) and f_{II} (%) on ψ is in accordance with the total exchange capacity, φ, of the [Nafion/$(SiO_2)_x$] composite membranes (Table 1). These findings confirm that the bending FT−IR vibrational peaks of water are diagnostic modes for the identification of the types of H_2O species and for the study of their interactions in bulk nanocomposite membranes. As expected the f_{III} (%) parameter shows that the water retention of the [Nafion/$(SiO_2)_x$] systems increases as the filler concentration increases.

The Raman spectra in the 1640−1590 cm^{-1} region (Figure 8) present the bending vibrations typical of low associated water species. In accordance with the investigation carried out for water in vapor phases, the doublet of bands at 1594 and 1625 cm^{-1}, shown in the insets of Figure 8a,b, was assigned correlatively to water species in dimer form, $(H_2O)_2$.[27,50−52] As expected, this latter species of water aggregates has the lowest possible dipolar moment. These characteristics lead us to hypothesize that these water dimer species represent the water aggregates located in the bulk environments of the material where the dielectric constant is low, i.e., near the hydrophobic Nafion host domains. Therefore, it is expected that water dimer species are dispersed in the hydrophobic channels with a diameter of 1−1.5 nm,[13] which interconnect the polar hydrophilic cages of [Nafion/$(SiO_2)_x$] composites.

Taken together, vibrational spectroscopy studies allowed us to conclude that the PTFE backbone domain in [Nafion/$(SiO_2)_x$] membranes adopts a 15/7 helical conformation independent of the SiO_2 concentration, and that the water in polar cages is distributed into three species. The bulk water, $[(H_2O)_n]$, increases as ψ rises, while the opposite behavior is revealed for both the bulk water domain associated with H_3O^+ ions and the water clusters involved in hydration of oxonium ions directly involved in the interaction with sulfonic acid groups. Furthermore, although the SiO_2 concentration does not affect the fluorocarbon backbone structure, it significantly influences the interactions of Nafion in polar clusters and the distribution of water domains in polar cages and in the interconnection channels. In particular, as ψ in the range $0 < \psi < 3.16$ rises, the increase in bulk water is to be ascribed to the hydrophilic character of the SiO_2 particle surface and to the increase in the total surface of the filler in bulk membranes.

3.4. Electrical Spectroscopy Studies. The electric response of the prepared membranes was investigated by Broadband Dielectric Spectroscopy (BDS) in the frequency and temperature ranges of 40 Hz−10 MHz and 5−135 °C, respectively.

A careful analysis of conductivity spectra performed as described elsewhere[36,53−55] allowed us to accurately measure the temperature dependence of σ_{DC} for [Nafion/$(SiO_2)_x$] membranes at 100% RH (Figure 11). Analysis of σ_{DC} profiles as a function of $1/T$ indicated that the [Nafion/$(SiO_2)_x$] systems exhibit three distinct conductivity regions, which are indicated as I, II, and III. In region I, σ_{DC} vs $1/T$ follows the typical Vogel−Tamman−Fulcher dependence,[53−55] thus demonstrating that segmental motions of polytetrafluoroethylene chains play a crucial role modulating the long-range charge-transfer mech-

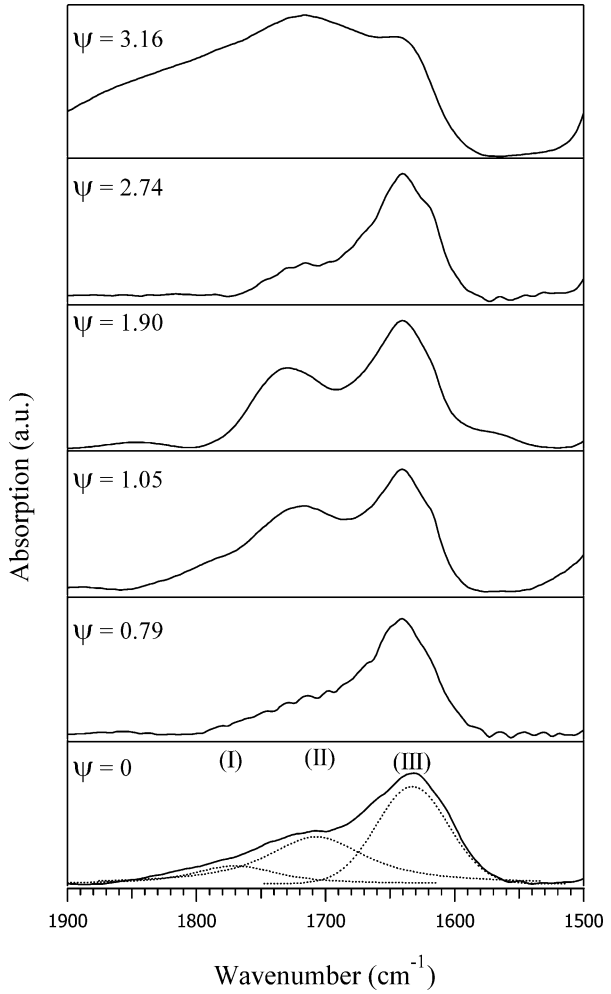

Figure 9. Decomposition by Gaussian functions of the MID FT−IR spectral range from 1500 to 1900 cm^{-1} for [Nafion/$(SiO_2)_x$] membranes.

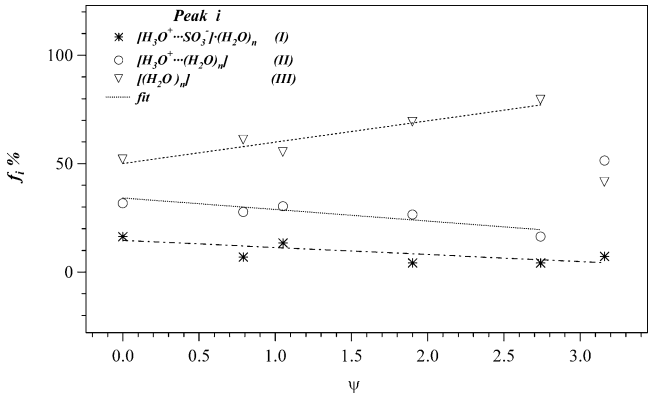

Figure 10. Percentages of different water species vs ψ. The semiquantitative percentage of each type of H_2O domain was determined with the formula f_i (%) = $A_i \cdot 100/\Sigma$, where A_i is the band area of a defined peak and $\Sigma = \sum_{i=1}^{3} A_i$. I, II, and III correspond to three different water domains.

anism of the obtained materials. Region II shows an Arrhenius-like dependence of σ_{DC} on $1/T$. It should be emphasized that the SiO_2 concentration has a significant effect on the electrical response of [Nafion/$(SiO_2)_x$] systems in region II, where a substantial decrease in conductivity is observed as ψ rises in the range 0−1.05. These findings are in accordance with the above thermal, mechanical, and vibrational spectroscopy analyses which showed that as ψ rises in the region $0 \leq \psi \leq 1.05$

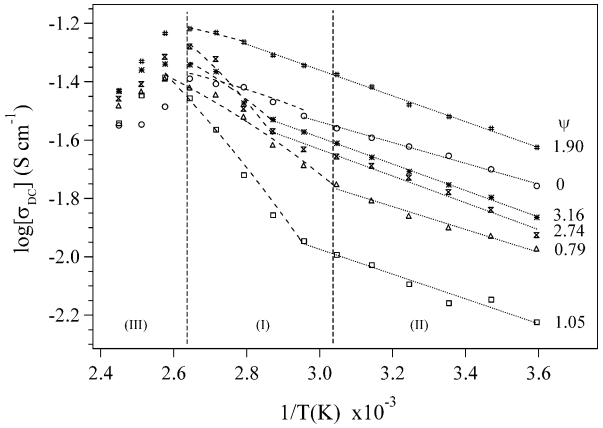

Figure 11. Dependence of σ_{DC} on the reciprocal of temperature for [Nafion/$(SiO_2)_x$] membranes. Conductivity regions I, II, and III are indicated. Dotted lines in I and II show VTF and Arrhenius-type fitted curves, respectively.

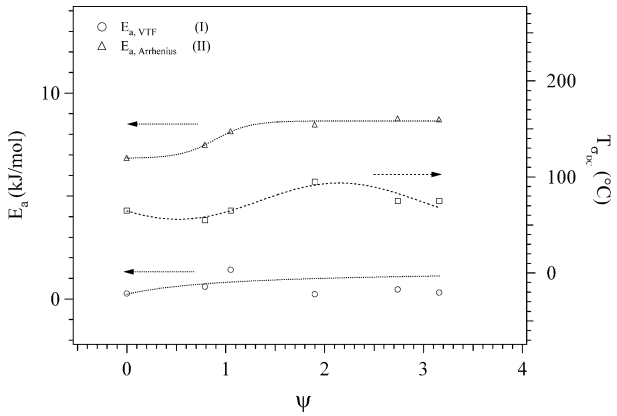

Figure 12. $E_{a,VTF}$ (I), $E_{a,Arrhenius}$ (II), and $T_{\sigma_{DC}}$ as a function of ψ. I and II indicate the conductivity regions.

the increase in the density of dynamic-cross-links between side acid groups of Nafion and SiO_2 oxocluster bridges limits the segmental motion of the fluorocarbon backbone, which in turn reduces the membranes conductivity values. In this region, the Arrhenius-like dependence of conductivity on temperature implies that segmental motion is not a crucial phenomenon for long-range proton-transfer mechanisms, which probably occur via hopping events between different cation coordination sites. Region III is characterized by a decrease in conductivity as temperature increases and shows that at high temperatures the influence of the (SiO_2 oxoclusters)−(acid side groups) cross-links on charge-transfer phenomena is negligible. Figure 12 presents the dependence of the VTF and Arrhenius-like activation energies, $E_{a,VTF}$ and $E_{a,Arrhenius}$, on ψ. It should be noted that in region II the activation energy for conduction is about 8 times higher than that in region I, thus indicating that the segmental motion of chains in region I plays a crucial role in regulating the proton charge-transfer mechanism, which is in agreement with the results described above. Furthermore, the decrease in conductivity in region II is easily explained if we consider that the SiO_2−Nafion side group interactions reduce the flexibility of both the backbone chains of hydrophobic domains and of polar clusters of Nafion.

In particular, $E_{a,VTF}$ is higher for samples with $\psi > 1$ than for those with $\psi < 1$. This information indicates that at $\psi > 1$, the increasing occupation volume of the inorganic filler hinders the segmental motion of fluorocarbon chains in polar cages. This behavior is also confirmed by the ideal glass transition

TABLE 4: Stability Range of Conductivity (SRC) and Conductivity at 105 °C and 100% RH for [Nafion/$(SiO_2)_x$] membranes.

ψ^a	SRC^b (°C)	conductivity at 105 °C (S cm^{-1})
0	$5 < T < 105$	4.0×10^{-2}
0.79	$5 < T < 115$	3.8×10^{-2}
1.05	$5 < T < 115$	3.4×10^{-2}
1.90	$5 < T < 105$	6.0×10^{-2}
2.74	$5 < T < 105$	5.2×10^{-2}
3.16	$5 < T < 115$	4.0×10^{-2}

[a] $\psi = \text{mol}_{SiO_2}/\text{mol}_{\cdot SO_3H}$. [b] SRC is the temperature range that at $T >$ 5 °C fulfills the following condition: $\{\partial \log(\sigma)\}/\{\partial(1/T)\} < 0$.

temperature (T_0) values, which show that increasing the inorganic component increases the temperature at which the configuration entropy of the system is zero, i.e., the material loses its nanometric homogeneity. Table 4 shows the conductivity of the [Nafion/$(SiO_2)_x$] materials at 105 °C and their Stability Range of Conductivity (SRC), which describes the temperature range that fulfils the equation $\partial(\ln \sigma_{DC})/\partial(1/T) < 0$. Table 4 confirms that the samples with broader SRCs are those with ψ in the range $0.79 < \psi \leq 1.05$.

We next investigated the conductivity mechanism in terms of relaxation events regulating the dynamics of [Nafion/$(SiO_2)_x$] materials by accurately measuring their broadband permittivity spectra.

Figure 13 shows the $\epsilon'(\omega)$ and $\epsilon''(\omega)$ spectra for two selected systems at various temperatures and over the entire frequency range investigated. Three spectral features are easily detected in the $\epsilon'(\omega)$ and $\epsilon''(\omega)$ profiles. At low frequencies the first decrease in $\epsilon'(\omega)$ corresponds to the effect of electrode polarization. In the medium-frequency range the second decrease in $\epsilon'(\omega)$, which in $\epsilon''(\omega)$ corresponds to a linear decrease with a slope of -1, is attributed to dc conduction. The third spectral region, located at the high-frequency end, is attributed to dielectric relaxations. This latter $\epsilon''(\omega)$ region presents relaxation peaks that shift through the frequency window as the temperature and sample composition change. A careful analysis of permittivity spectra was carried out by using the empirical equation[53−57]

$$\epsilon^*(\omega) = \epsilon_\infty + \sum_\infty \frac{\Delta\epsilon_k}{\{1 + (i\omega\tau)^{\alpha_k}\}^{\beta_k}} + \frac{\sigma_{DC}\cdot(i\omega\tau_{el})^{\gamma}}{i\omega[1 + (i\omega\tau_{el})^{\gamma}]} \quad (1)$$

where σ_{DC} is the dc conductivity, α_k and β_k are shape parameters describing the symmetric and asymmetric broadening of the kth relaxation peak, $\tau_k = (2\pi f_k)^{-1}$ is the dielectric relaxation time (f_k in Hz is the frequency of the peak maximum), $\Delta\epsilon_k$ is the relaxation strength, and τ_{el} is the relaxation time associated with the electrode polarization phenomena.

Equation 1 was used because the first two terms simulate the dielectric relaxations of the materials very well, while the third term accounts for the electrode polarization phenomena and dc conductivity. As reported elsewhere,[53−57] to obtain accurate fits of the dielectric spectra, we used the σ_{DC} and τ_{el} values measured in the Cole−Cole representation of the low-frequency conductivity and permittivity profiles, respectively. Fixing these latter parameters in the third term of eq 1 allowed us to subtract the dc conduction and polarization phenomena from the total permittivity profiles. The pure dielectric permittivity spectra thus determined are shown in Figure 14 for selected samples. Figure 15 shows the $\epsilon''(\omega)$ profiles before (Figure 15a) and after (Figure 15b) subtraction of σ_{DC} and electrode polarization contributions. Figure 15b reports a typical fit of the two revealed relaxation peaks. The low-frequency peak was attributed to the α-relaxation mode, and the peak at higher frequencies was attributed to the β-relaxation mode of [Nafion/$(SiO_2)_x$] materials.

To elucidate the materials' charge transport mechanism and bulk relaxation events, we carefully examined the fitting parameters of α- and β-relaxations determined with eq 1 in relation to sample temperature and composition.

Results shown in Figure 16 confirmed the presence of three relaxation regions for the [Nafion/$(SiO_2)_x$] systems. Therefore, as expected, the behavior of the dependence of the logarithms

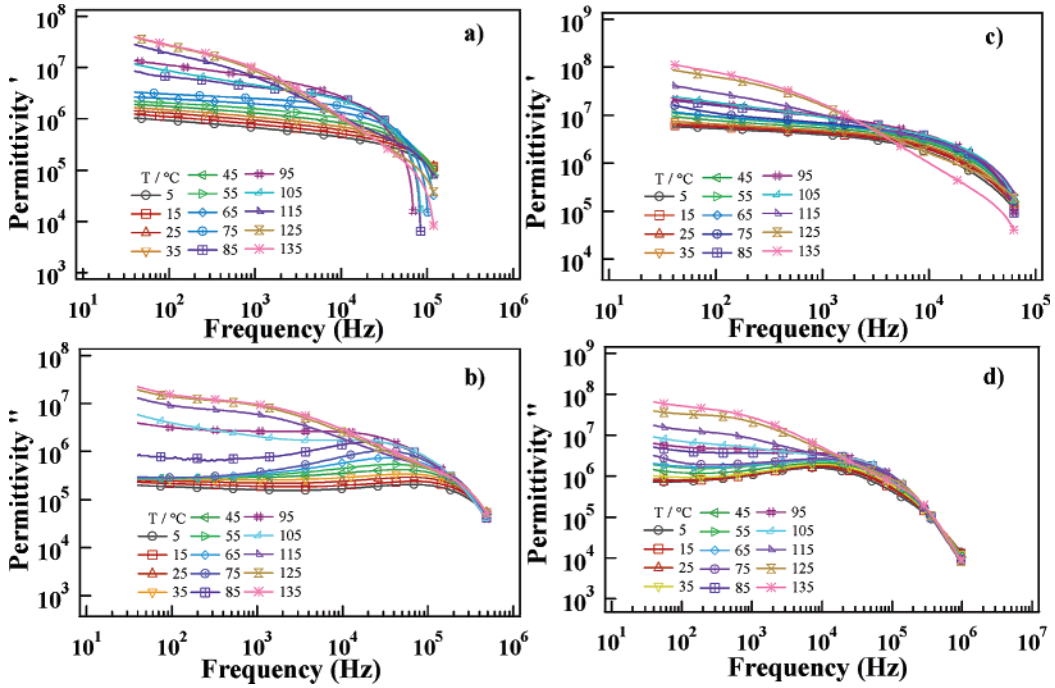

Figure 13. Selected real and imaginary permittivity spectra for [Nafion/$(SiO_2)_x$] membranes with varying frequency and temperature: (a and b) $\psi = 0$; (c and d) $\psi = 1.90$.

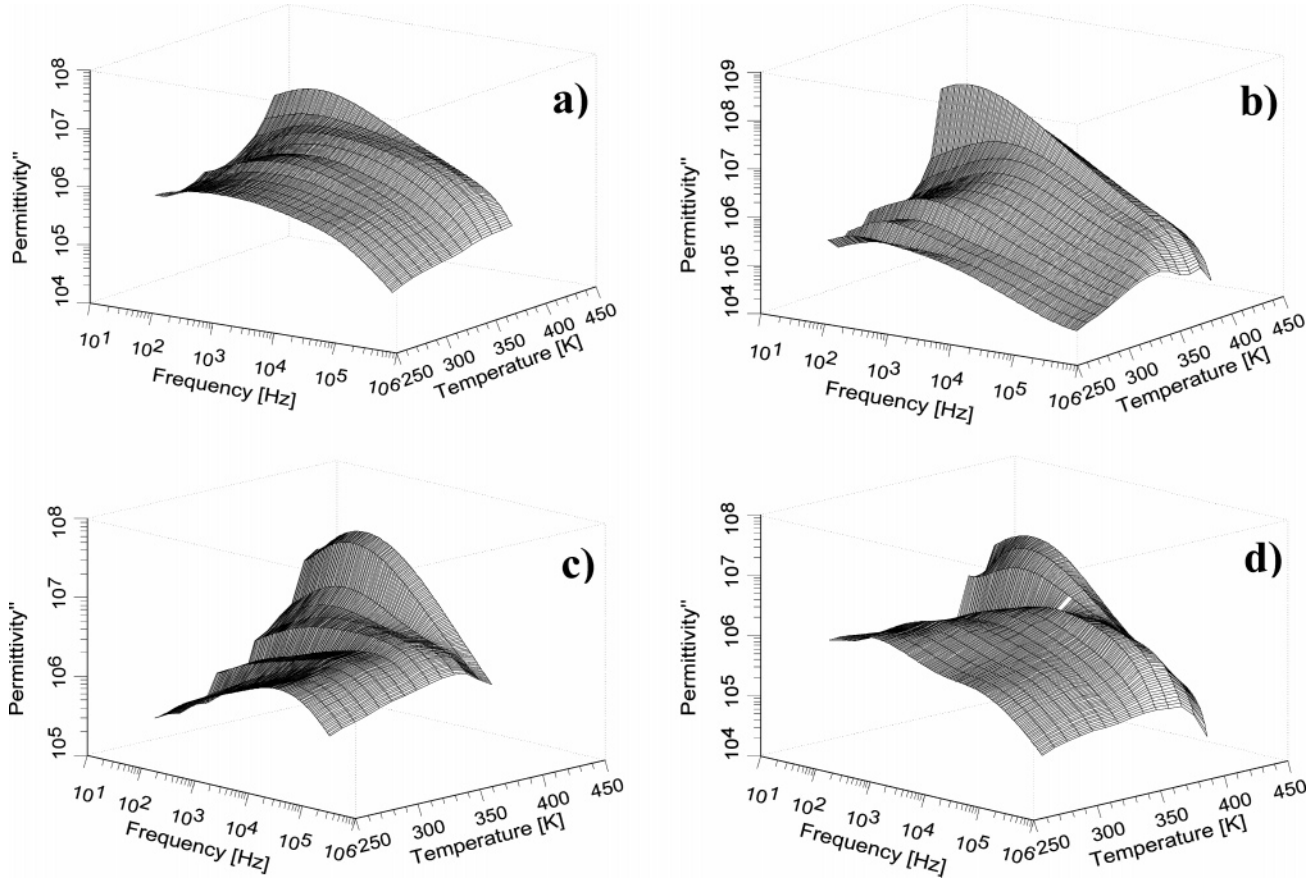

Figure 14. Imaginary component of dielectric spectra for selected [Nafion/$(SiO_2)_x$] membranes after subtraction of σ_{DC} and electrode polarization contributions: (a) $\psi = 0$; (b) $\psi = 0.79$; (c) $\psi = 1.90$; and (d) $\psi = 2.74$.

of the relaxation peak frequency on temperature was of Vogel−Tamman−Fulcher−Hesse (VTFH)[58] type for the α-relaxation mode and Arrhenius-like for the β-event, thus confirming the attribution given above. α is the relaxation mode associated with the segmental motion of the host polymer. This relaxation process, which is also defined as the "dynamic glass transition" process, takes into account the segmental motions of the fluorocarbon backbone chains caused by diffusion of the rotational conformational states[58,59] of chains located in dense hydrophobic environments of Nafion. The f_α vs $1/T$ data curves of regions I and II are shown in Figure 16. These curves were satisfactorily fitted by using the VTFH curvilinear dependence:[58,59]

$$\ln f_{\text{peak},\alpha} = \ln f_{\infty,\alpha} - \frac{E_\alpha}{R(T - T_0)} \qquad (2)$$

where $f_{\infty,\alpha}$ is a pre-exponential factor, E_α is the activation energy, and T_0 is the ideal thermodynamic glass transition temperature.

The β-relaxation mode is associated with local motions resulting from the rotational fluctuations of Nafion acid side groups or parts of them. The Arrhenius-like equation used to fit the linear dependence of f_β on temperature (Figure 16) is[58,59]

$$\ln f_{\text{peak},\beta} = \ln f_{\infty,\beta} - E_\beta/RT \qquad (3)$$

where $f_{\infty,\beta}$ is the pre-exponential factor and E_β is the activation energy.

Figure 17 reports the plots of the activation energies vs ψ determined in regions I and II by fitting the frequencies of α and β relaxation modes with eqs 2 and 3, respectively. It should be noted that the α relaxation mode in regions I and II presents activation energy values which are 1 order of magnitude lower than those of β relaxation. In region II the dependence of E_β and E_α on ψ shows a monotonic exponential decrease, reaching a plateau at $\psi \geq 2$. Considering that II is the region in which the interactions of Nafion polar side groups with SiO_2 nanofillers present the strongest intensity and that the profile of the dependence of the storage modulus on ψ exhibits a curve that is similar to that of E_β and E_α, we can propose that in region II the dynamic cross-links between sulfonic groups and the SiO_2 filler are of crucial importance in regulating the materials' mechanical and electrical properties. Results confirm that the density of cross-links between Nafion side groups and SiO_2 oxoclusters in the membranes increases as ψ decreases and reaches a critical value for $\psi > 1.9$. These observations suggest that at $\psi > 1.9$, SiO_2 clusters embedded in [Nafion/$(SiO_2)_x$] composites could be distinguished in two different classes depending on two different types of interactions they participate in within the polar environment cages of the bulk membranes. The first class (A) accounts for the amount of SiO_2 that is predominantly implicated in dynamic cross-links, in other words, the silica clusters interacting with the Nafion polar side groups. The second class (B) corresponds to silica moieties interacting predominantly with other surrounding oxoclusters. B acts as a filler and influences the material due to the fraction of its volume hindrance in the bulk membranes. It is noteworthy that as the amount of B in bulk [Nafion/$(SiO_2)_x$] composites increases, the nanometric homogeneity of the materials is lost, thereby giving so rise to a biphasic system. It should be pointed out that the amount of SiO_2 of the A type depends on the concentration of acid side groups in the Nafion host polymer. Results support the hypothesis that at $\psi > 1.9$ a considerable amount of B

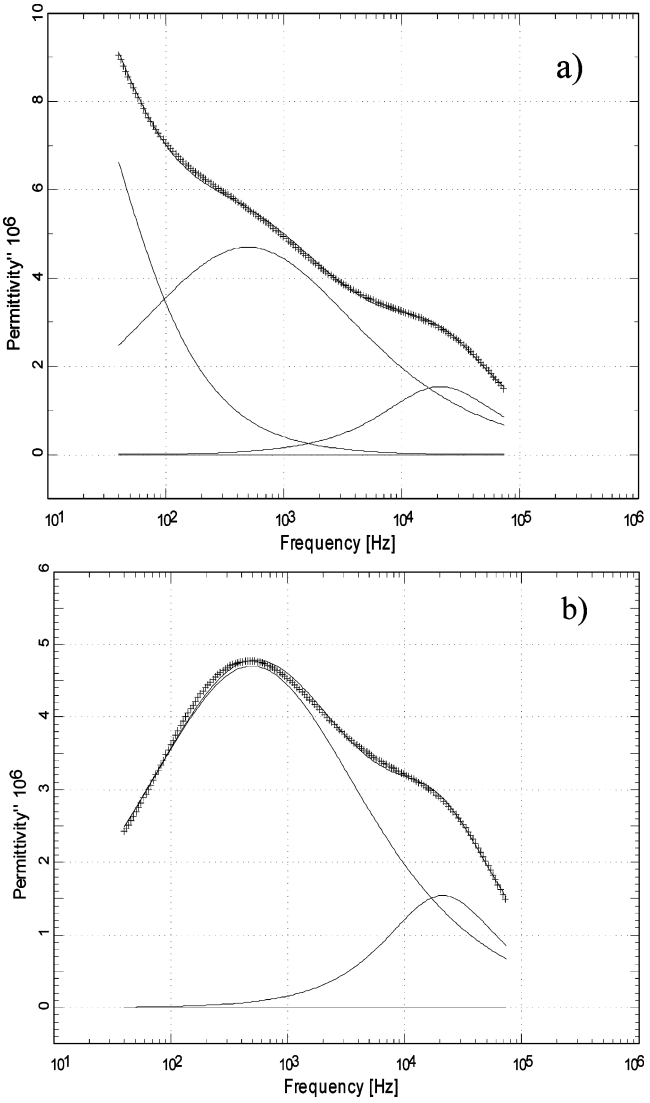

Figure 15. Imaginary components of the dielectric spectrum of [Nafion/$(SiO_2)_x$] membrane with $\psi = 1.90$. Panel a: dielectric loss spectrum fitted with eq 1. Panel b: difference dielectric loss spectrum obtained by subtracting the spectral contribution of electrode polarization and σ_{DC} from the electric spectrum in panel a.

nanodomains are formed in polar cages of [Nafion/$(SiO_2)_x$] membranes. These considerations explain the observation that the mechanical properties and the activation energies of β and α relaxation in the second region increase exponentially as ψ decreases.

Further support for this interpretation of the data is provided by the plots of ΔH_I dependence on ψ shown in Figure 3, which demonstrate that the endothermic enthalpy of peak I, corresponding to the order−disorder molecular rearrangements inside Nafion polar clusters, rises as ψ increases for $\psi \leq 1.9$. These results prove that the thermal stability and SRC increase as a consequence of the predominant effect of A type silica in [Nafion/$(SiO_2)_x$] membranes. Furthermore, a comparison of E_α and E_β (Figure 17) with the activation energies for conduction (Figure 12) reveals the following: (a) in region I the conductivity of the [Nafion/$(SiO_2)_x$] materials is regulated exclusively by the segmental motion of the fluorocarbon backbone; indeed the values for $E_{a,VTF}$(I) and $E_{\alpha,I}$ are quite co-incident; and (b) in region II both segmental motions of the fluorocarbon backbone and molecular relaxation of side groups involved in dynamic cross-links seem to regulate the proton-transfer mechanisms

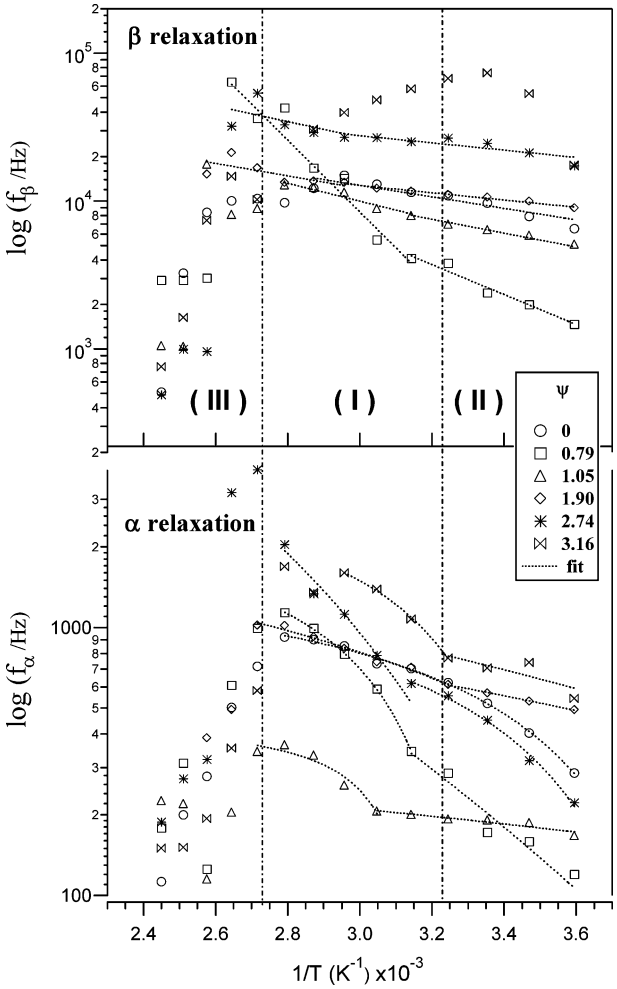

Figure 16. Dependence of f_α and f_β on the reciprocal of temperature in [Nafion/$(SiO_2)_x$] membranes. Regions I, II, and III are indicated.

($E_{\beta,II} \approx E_{a,Arrhenius}$ (II) and $E_{\beta,II} \gg E_{\alpha,II}$). These findings prompt us to affirm that in region II segmental motion of the fluorocarbon backbone and side group dynamics are strongly coupled with each other.

Further support for this interpretation of the data is provided by plots of the dependence of $\Delta\epsilon_\alpha$ and $\Delta\epsilon_\beta$ on temperature (Figure 18). In region II the intensities of $\Delta\epsilon_\alpha$ and $\Delta\epsilon_\beta$ are on the same order of magnitude, while in region I, $\Delta\epsilon_\alpha$ is at least of 1 order of magnitude higher than $\Delta\epsilon_\beta$. In addition, $\Delta\epsilon_\alpha$ increases with increasing temperature, thus confirming that α relaxation of the fluorocarbon backbone is strongly correlated with the dynamics of side groups. It seems that this temperature dependence results from cross-correlation terms to $\langle\mu^2\rangle$ between the fluorocarbon backbone and side groups relaxations, which become more important as the temperature increases.

For β relaxation, because the main dipole moment is located in the side group, it is expected that even small fluctuations of the side group would contribute significantly to the dielectric loss. An accurate analysis of the plots obtained for pristine Nafion shown in Figure 18 indicates that in both I and II regions (a) for ψ in the region $0 \leq \psi \leq 1.05$, a decrease in $\Delta\epsilon_\beta$ is observed, (b) for $\psi = 1.9$, $\Delta\epsilon_\beta$ is independent of temperature and presents the highest value, and (c) for $\psi > 1.9$, a decrease in $\Delta\epsilon_\beta$ is registered. On this basis we could conclude that the [Nafion/$(SiO_2)_x$] complex with $\psi = 1.9$ presents the best conductivity owing to the stronger coupling between the fluorocarbon backbone and the moving dipoles of side groups in the Nafion backbone host polymer.

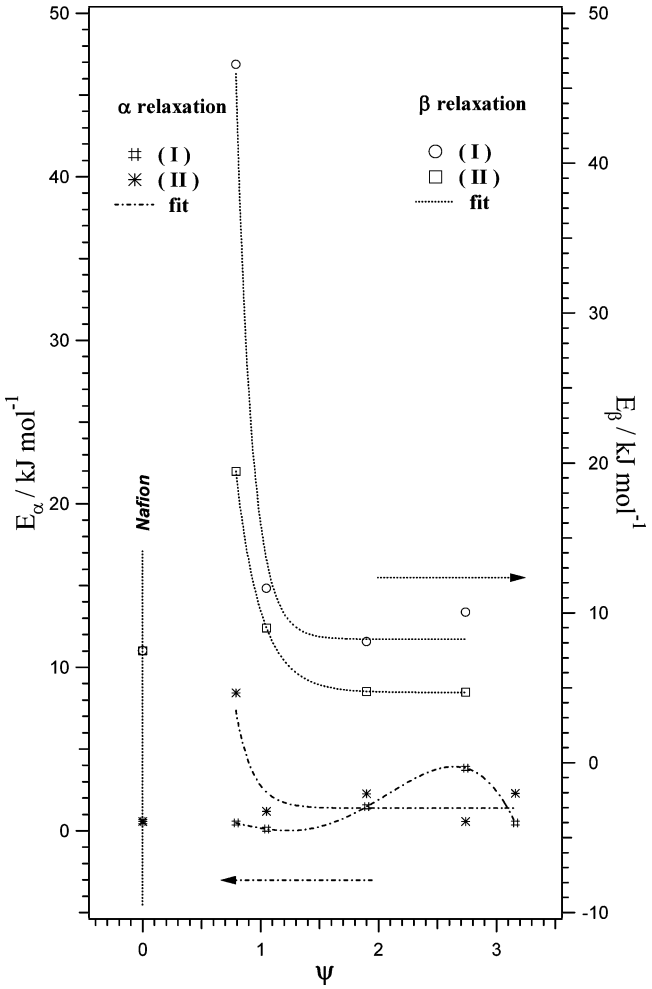

Figure 17. E_α and E_β in regions I and II as a function of ψ.

Information on the molecular dynamics and coupling phenomena between relaxation modes in the polymer materials was also provided by the study of the shape parameters m and n, where $m = \alpha_k$ and $n = \alpha_k\beta_k$, with α_k and β_k fitting parameters of α and β loss-peaks simulated by eq 1. Figure 19 shows that, with the exception of the [Nafion/$(SiO_2)_x$] material with $\psi = 0.79$, the shape parameters for α loss-peak yield a value of ~0.65 for both n and m. In accordance with the literature,[58,59] the shape parameters of α relaxations depend on the temperature and cross-linking density. The values of n and m become narrower with increasing temperature and broaden considerably with cross-linking processes. An α relaxation n close to 0.5 is typical of polymer materials in which the local chain dynamics of polymer backbone segments are influenced by the environment.[58,59] The shape parameter m_α varies with the intermolecular interactions. In general, when the intermolecular interactions decrease in strength the value of m increases up to 1. In Figure 19a, the m_α values for [Nafion/$(SiO_2)_x$] membranes are close to ~0.65, revealing very strong intermolecular coupling between the motion of fluorocarbon chains in hydrophobic domains and dynamics of side chain groups in polar clusters of the Nafion host polymer. For these reasons, the decrease in m_α also accounts for the cross-linking phenomena which occur in the polar clusters of the Nafion host polymer. Figure 19b shows that parameters n_β and m_β of β relaxation, which range from 0.6 to 1, could be related to local motions of acid side groups hindered by the cross-linking processes. These results, together with the vibrational characterizations, allow us to conclude that the conductivity of the [Nafion/$(SiO_2)_x$] materials is mainly regulated

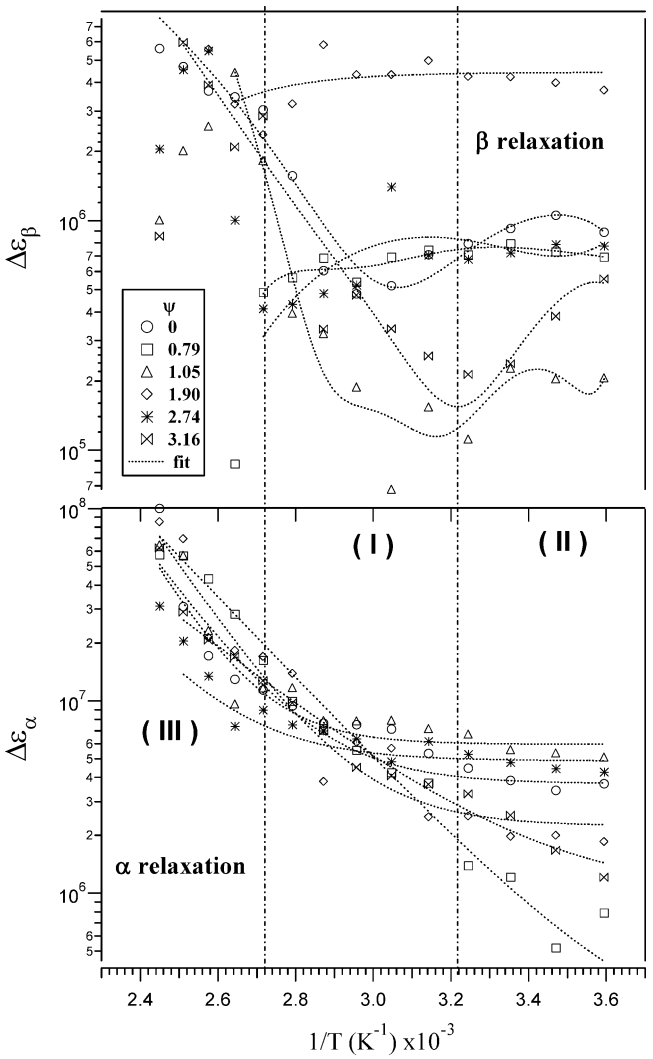

Figure 18. Dependence of the relaxation strengths, $\Delta\epsilon_\alpha$ and $\Delta\epsilon_\beta$, on the reciprocal of temperature. Regions I, II, and III are indicated.

by segmental motion of fluorocarbon chains and by the SiO_2 concentration. The effect of silica on conductivity is crucial for stabilizing the hydrophobic and the hydrophilic domains and for modulating proton charge transfer in both the polar hydrophilic clusters and the channels interconnecting the hydrophilic cages.

Taken together, the results of BDS, MDSC, and DMA investigations demonstrate that the physical properties of Nafion and [Nafion/$(SiO_2)_x$] composite membranes are regulated by two different host polymer relaxation events whose dynamics are strongly coupled to each other. The first relaxation phenomenon R_c is the cage relaxation, which deals with the molecular relaxations occurring inside the polar cages of Nafion-based materials, and is revealed in terms of (a) the mechanical α-relaxation in DMA measurements, (b) the dielectric β-relaxation in BDS measurements, and (c) the endothermic peak I in MDSC profiles. The second event R_{fd}, which is related to the relaxation of fluorocarbon domains of the Nafion host polymer, is revealed in terms of (a) dielectric α-relaxation in permittivity spectra and (b) mechanical β-relaxation in real and imaginary components of E^*.

Finally, we can hypothesize that proton migration inside polar clusters and their interconnecting channels probably occurs owing to a proton hopping process that is tightly regulated by the concentration of interstitial free water, the number density of acid side groups $-SiO_2$ cross-links, and the segmental motion

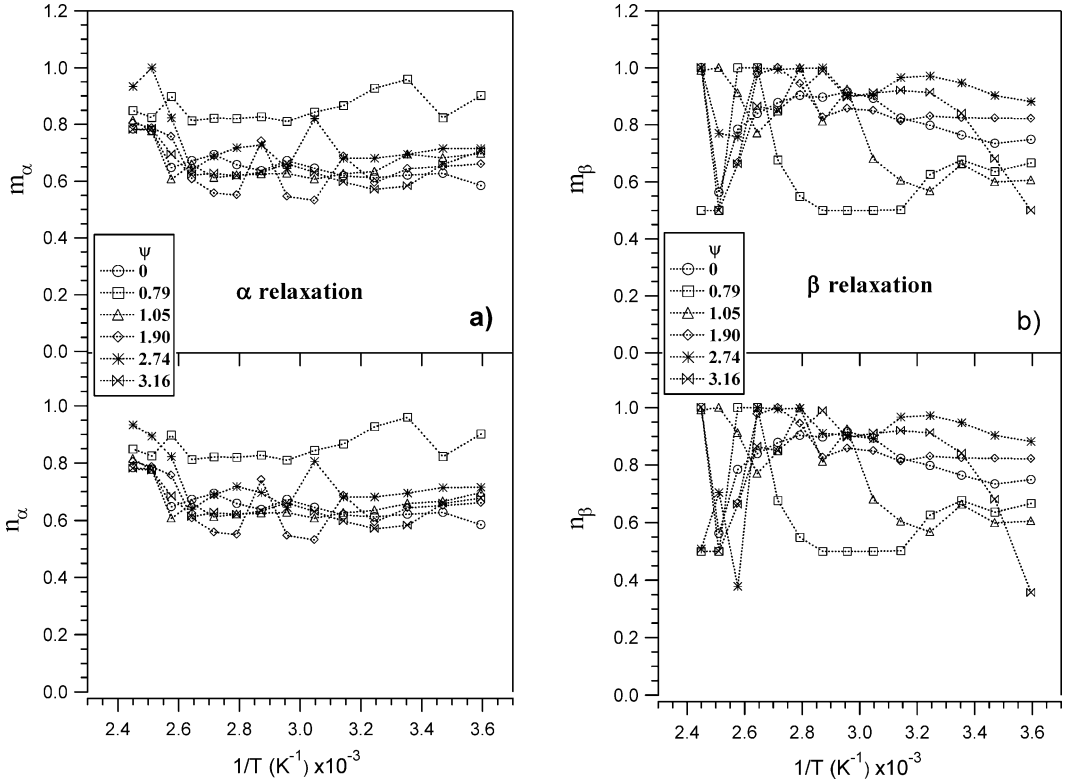

Figure 19. Dependence of the shape parameters *m* and *n* on the reciprocal of temperature for α- and *β*-modes (panels a and b, respectively).

of the fluorocarbon backbone. Therefore, the conductivity mechanism of [Nafion/$(SiO_2)_x$] membranes could be classified as a *peristaltic*-like process. This long-range charge migration takes place successfully when two or more different water domains contact each other. These water contacts form as a result of the above-described molecular relaxation events of the host material, which cause the water domains to broaden and shrink, thus continuously changing their shape. This process gives rise to a new intermediate intersection water volume in which the probability of exchanging a proton between different water domains by hopping processes is very high. It should be highlighted that this *peristaltic*-like process requires strong coupling between the relaxation movements of PTFE domains and the acid side groups of the Nafion host polymer. The proposed mechanism is supported by the following data: (a) the activation energy for R_{fd} is ca. 3 kJ/mol, i.e., close to that of $RT = 2.48$ kJ/mol at 298 K; (b) R_{fd} is strongly coupled with R_c, whose activation energy is 1 order of magnitude higher than that of R_{fd}; and (c) the conductivity is easily stimulated thermally and presents values typical of high conducting polymer electrolytes, indicating that charge-transfer processes occur with migration times and diffusion coefficients in the range expected for polymer chain dynamics.

4. Conclusions

This report presents the results of studies devoted to the elucidation of the effect of SiO_2 nanopowders on the structure, properties, and conductivity mechanism of [Nafion/$(SiO_2)_x$] nanocomposite membranes. The films were prepared by a solvent casting procedure, using a precursor solution obtained by suspending nanopowders of fumed silica having a crystallite size of less than 70 nm in a 5 wt % Nafion solution. The solvent casting method, performed at 80 °C, yielded six transparent and homogeneous membranes with the formula [Nafion/$(SiO_2)_x$], where $0 \leq x \leq 15$ wt %; the membranes had a thickness of less than 300 μm.

Thermal analyses (TG and MDSC) showed that the [Nafion/$(SiO_2)_x$] membranes are stable up to 170 °C. The thermal stability of the materials increases slightly as ψ increases in the region $0 \leq \psi \leq 1.9$. Thermal transitions I, II, and III were detected in the MDSC profiles from 90 to 300 °C. Endothermic event I is associated with an order−disorder transition linked to the polymer relaxation processes inside the Nafion polar clusters, II was attributed to the decomposition of SO_3H groups, and III to an order−disorder process of fluorocarbon microcrystalline regions of the Nafion polymer. Results showed that when $0 \leq \psi < 1.9$, $^-SO_3H-SiO_2$ interactions increase the crystallinity of PTFE domains of the Nafion moiety. These interactions improve the thermal stability of $^-SO_3H$ groups, and hinder the relaxation events in the hydrophilic dipolar interaction clusters of the Nafion host polymer.

ESEM and EDAX measurements showed that the membranes are homogeneous materials with very smooth surfaces.

Vibrational studies (FT−IR and FT−Raman) of the membranes allowed us to conclude that their hydrophobic domains consist of PTFE fluorocarbon chains in a helical conformation with a $D(14\pi/15)$ symmetry. Four different species of water domains were detected: bulk water $[(H_2O)_n]$; water present as hydrated oxonium ions directly associated with $[H_3O^+\cdots SO_3^-]\cdot(H_2O)_n$ sulfonic anion groups; water associated with H_3O^+ $[H_3O^+\cdots(H_2O)_n]$; and water molecules in dimer form $[(H_2O)_2]$. The latter two species of water are present in both the Nafion hydrophilic polar cages and their interconnecting channels. The concentration of each water species is modulated by the SiO_2 concentration in the membranes. SiO_2 was also found to significantly influence the $SiO_2-HSO_3^-$ interactions in hydrophilic polar clusters.

DMA investigations revealed the presence of two distinct mechanical relaxation events in Nafion and [Nafion/$(SiO_2)_x$] membranes. The mechanical α-mode, associated with relaxation in the cluster aggregates of Nafion side chains, was detected at

100 °C, while β-relaxation, attributed to the main-chain motions in fluorocarbon domains, was revealed at ca. 19 °C.

The electric response of the membranes was investigated by Broadband Dielectric Spectroscopy (BDS) in the frequency and temperature range of 40 Hz−10 MHz and 5−135 °C, respectively. Analysis of the BDS spectra revealed the presence of two different dielectric relaxation phenomena in [Nafion/$(SiO_2)_x$] membranes. The low-frequency relaxation event is attributed to the α-relaxation mode of PTFE backbone domains in Nafion, while that detected at high frequencies corresponds to the β-relaxation mode of Nafion side chains bearing the sulfonic acid groups. Both these dielectric modes are strongly coupled with each other and are diagnostic for the effect of the SiO_2 concentration on the properties of [Nafion/$(SiO_2)_x$] membranes.

Results allow us to affirm that the membranes' SiO_2 oxo-clusters modulate the relaxations of both the hydrophobic and hydrophilic components of the Nafion polymer host. At $\psi <$ 1.9, the stability range of conductivity (SRC) and the conductivity values within SRC depend on the SiO_2 concentration. In particular, the silica nanofiller modifies the properties of the membranes owing to the formation of dynamic cross-links with acid side groups of Nafion which influence the macromolecular dynamics of the Nafion polymer host. It should be noted that the membrane doped with 9 wt % SiO_2 has a conductivity value of 6.0×10^{-2} S·cm^{-1} at 105 °C and 100 RH %.

Finally, it should be highlighted that the combined studies carried out simultaneously by DMA, MDSC, and BDS techniques allowed us to determine that the charge-transfer mechanism in [Nafion/$(SiO_2)_x$] materials is driven by two relaxation phenomena which are diagnostic for the properties and interactions occurring in the bulk materials. The first event, termed R_c, deals with the relaxation mode of polar ion cages of membranes and was studied through a detailed analysis of (a) the mechanical α-relaxation in DMA spectra, (b) the endothermic peak I in MDSC measurements, and (c) the dielectric β-relaxation in permittivity spectra. The second phenomenon, termed R_{fd}, describes the dynamics of fluorocarbon backbone polymer chains located in hydrophobic domains of Nafion, and could be followed by analyzing the dielectric α-relaxation in permittivity spectra and the mechanical β-relaxation in real and imaginary components of E^*.

In conclusion, we propose that proton migration along interconnecting channels and polar hydrophilic clusters takes place owing to proton exchange processes modulated by the amount and types of interstitial water domains, the density of hybrid $SiO_2-(HSO_3)^-$ cross-links, and the segmental motions of the fluorocarbon backbone of Nafion polymer. This in turn leads to the hypothesis that the exchange of protons between different fluctuating water species domains occurs through hopping processes, and that this mechanism is strongly regulated by the molecular relaxation events in the materials.

Acknowledgment. Research was funded by the Italian MURST project NUME of FISR2003, "Sviluppo di membrane protoniche composite e di configurazioni elettrodiche innovative per celle a combustibile con elettrolita polimerico".

References and Notes

(1) Larminie, J.; Dicks, A. *Fuel Cell System Explained*; J. Wiley and Sons: Chichester, UK, 2000.

(2) Ogden, J. M. In *Handbook of Fuel Cells*: *Fundamentals, Technology and Applications*; Vielstich, W., Lamm, A., Gasteiger, H. A., Eds.; Wiley: Chichester, UK, 2003; Vol. 3, p 3.

(3) Theisen, T. In *Handbook of Fuel Cells*: *Fundamentals, Technology and Applications*; Vielstich, W., Lamm, A., Gasteiger, H. A., Eds.; Wiley: Chichester, UK, 2003; Vol. 3, p 25.

(4) Appleby, A. J. *Sci. Am.* **1999**, *281*, 74.

(5) Cleghorn, S. J. C.; Ren, X.; Springer, T. E.; Wilson, M. S.; Zawodzinski, C.; Zawodzinski, T. A.; Gottesfeld, S. *Int. J. Hydrogen Energy* **1997**, *22*, 1137.

(6) Kunz, H. R.; Gruver, G. A. *J. Electrochem. Soc.* **1975**, *122*, 1279.

(7) Huang, J. C.; Sen, R. K.; Yeager, E. *J. Electrochem. Soc.* **1979**, *126*, 786.

(8) Thompsett, D. In *Handbook of Fuel Cells*: *Fundamentals, Technology and Applications*; Vielstich, W., Lamm, A., Gasteiger, H. A., Eds.; Wiley: Chichester, UK, 2003; Vol. 3, p 467.

(9) Tado, T. In *Handbook of Fuel Cells*: *Fundamentals, Technology and Applications*; Vielstich, W., Lamm, A., Gasteiger, H. A., Eds.; Wiley: Chichester, UK, 2003; Vol. 3, p 481.

(10) Rikukawa, M.; Sanui, K. *Prog. Polym. Sci.* **2000**, *25*, 1463.

(11) Kreuer, K. D. *J. Membr. Sci.* **2001**, *185*, 29.

(12) Alberti, G.; Casciola, M. *Solid State Ionics* **2001**, *145*, 3.

(13) Mauritz, K. A.; Moore, R. B. *Chem. Rev.* **2004**, *104*, 4535.

(14) Alberti, G.; Casciola, M.; Massinelli, L.; Bauer, B. *J. Membr. Sci.* **2001**, *185*, 73.

(15) Kocha, S. S. In *Handbook of Fuel Cells*: *Fundamentals, Technology and Applications*; Vielstich, W., Lamm, A., Gasteiger, H. A., Eds.; Wiley: Chichester, UK, 2003; Vol. 3, p 538.

(16) Neergat, M.; Friedrich, K. A.; Stimming, U. In *Handbook of Fuel Cells*: *Fundamentals, Technology and Applications*; Vielstich, W., Lamm, A., Gasteiger, H. A., Eds.; Wiley: Chichester, UK, 2003; Vol. 4, p 856.

(17) Nakao, M.; Yoshitake, M. In *Handbook of Fuel Cells*: *Fundamentals, Technology and Applications*; Vielstich, W., Lamm, A., Gasteiger, H. A., Eds.; Wiley: Chichester, UK, 2003; Vol. 3, p 412.

(18) Alberti, G.; Casciola, M. *Annu. Rev. Mater. Res.* **2003**, *33*, 129.

(19) Mauritz, K. A. *Mater. Sci. Eng. C* **1998**, *6*, 121.

(20) Honma, I.; Nakajima, H.; Nishikawa, O.; Sugimoto, T.; Nomura, S. *Solid State Ionics* **2003**, *162*, 237.

(21) Di, Noto, V.; Vittadello, M. *Electrochim. Acta* **2005**, *50*, 3998.

(22) Di, Noto, V.; Vittadello, M.; Jayarkody, R. P. J.; Khalfan, A. N.; Greenbaum, S. G. *Electrochim. Acta* **2005**, *50*, 4007.

(23) Zawodzinski, T. A.; Derouin, C.; Radzinski, S.; Sherman, R. J.; Smith, V. T.; Springer, T. E.; Gottesfeld, S. *J. Electrochem. Soc.* **1993**, *140*, 1041.

(24) Fontanella, J. J.; Edmondson, C. A.; Wintersgill, M. C.; Wu, Y.; Greenbaum, S. G. *Macromolecules* **1996**, *29*, 4944.

(25) Fontanella, J. J.; McLin. M. G.; Wintersgill, M. C. *J. Polym. Sci. B*: *Polym. Phys.* **1994**, *32*, 501.

(26) Paddison, S. J. *Annu. Rev. Mater. Res.* **2003**, *33*, 289.

(27) Laporta, M.; Pegoraro, M.; Zanderighi, L. *Phys. Chem. Chem. Phys.* **1999**, *1*, 4619.

(28) Falk, M. *Can. J. Chem.* **1980**, *58*, 1495.

(29) Quezado, S.; Kwak, J. C. T.; Falk, M. *Can. J. Chem.* **1984**, *62*, 958.

(30) Ludvigsson, M.; Lindgren, J.; Tegenfeldt, J. *Electrochim. Acta* **2000**, *45*, 2267.

(31) Mauritz, K. A.; Stefanithis, I. D.; Davis, S. V.; Scheetz, R. W.; Pope, R. K.; Wilkes, G. L.; Huang, H. H. *J. Appl. Polym. Sci.* **1995**, *55*, 181.

(32) Adjemian, K. T.; Srinivasan, S.; Benuziger, J.; Bocarsly, A. B. *J. Power Sources* **2002**, *109*, 356.

(33) Popall, M.; Du, X. M. *Electrochim. Acta* **1995**, *40*, 2305.

(34) Staiti, P.; Aricò, A. S.; Baglio, V.; Lufrano, F.; Passalacqua, E.; Antonucci, V. *Solid State Ionics* **2001**, *145*, 101.

(35) Shao, Z. G.; Xu, H.; Li, M.; Hsing, I. M. *Solid State Ionics* **2006**, *177*, 779.

(36) Di, Noto, V.; Vittadello, M.; Zago, V.; Pace, G.; Vidali, M. *Electrochim. Acta* **2006**, *51*, 1602.

(37) De Almeida, S. H.; Kawano, Y. *J. Therm. Anal. Calorim.* **1999**, *58*, 569.

(38) Young, S. K.; Mauritz, K. A. *J. Polym. Sci. B*: *Polym. Phys.* **2001**, *39*, 1282.

(39) Prud'Homme, K. *Electronic Material Handbook*; ASTM International: Materials Park, OH, 1989; Vol. 1, p 838.

(40) Di, Noto, V. *J. Phys. Chem. B* **2000**, *104*, 10116.

(41) Hannon, M. J.; Boerio, F. J.; Koenig, J. L. *J. Chem. Phys.* **1969**, *50*, 2829.

(42) Koenig, J. L.; Boerio, F. J. *J. Chem. Phys.* **1969**, *50*, 2823.

(43) Moynihan, R. E. *J. Am. Chem. Soc.* **1959**, *81*, 1045.

(44) Liang, C. Y.; Krimm, S. *J. Chem. Phys.* **1956**, *25*, 563.

(45) Gruger, A.; Régis, A.; Schmatko, T.; Colomban, P. *Vib. Spectrosc.* **2001**, *26*, 215.

(46) Liang, Z. X.; Chen, W. M.; Liu, J.G.; Wang, S. L.; Zhou, Z. H.; Li, W. Z.; Sun, G. Q.; Xin, Q. *J. Membr. Sci.* **2004**, *233*, 39.

(47) Ludvigsson, M.; Lindgren, J.; Tegenfeldt, J. *Electrochim. Acta* **2000**, *45*, 2267.

(48) Etchepare, J. *Spectrochim. Acta A* **1970**, *26*, 2147.

(49) Di, Noto, V.; Damioli, P.; Vittadello, M.; Dall'Igna, R.; Boella, F. *Electrochim. Acta* **2003**, *48*, 2329.

(50) Ford, T. A.; Falk, M. *Can. J. Chem.* **1968**, *46*, 3579.
(51) Bertie, J. E.; Ahmed, K.; Eysel, H. H. *J. Phys. Chem.* **1989**, *93*, 2210.
(52) Falk, M. *Spectrochim. Acta, Part A* **1984**, *40*, 43.
(53) Vittadello, M.; Suarez, S.; Fujimoto, K.; Di, Noto, V.; Greenbaum, S. G.; Furukawa, T. *J. Electrochem. Soc.* **2005**, *152*, A956.
(54) Di, Noto, V. *J. Phys. Chem. B* **2002**, *106*, 11139.
(55) Di, Noto, V.; Vittadello, M.; Greenbaum, S. G.; Suarez, S.; Kano, K.; Furukawa, T. *J. Phys. Chem. B* **2004**, *108*, 18832.
(56) Furukawa, T.; Imura, M.; Yuruzume, H. *Jpn. J. Appl. Phys.* **1997**, *36*, 1119.
(57) Kano, K.; Takahashi, Y.; Furukawa, T. *Jpn. J. Appl. Phys.* **2001**, *40*, 3246.
(58) Schönhals, A. In *Dielectric Spectroscopy of Polymeric Materials*; Runt, J. P., Fitzgerald, J. J., Eds.; American Chemical Society: Washington, DC, 1997; p 81.
(59) Schönhals, A. In *Broadband Dielectric Spectroscopy*; Kremer, F., Schönhals, A., Eds.; Springer-Verlag: Berlin, Germany, 2003; p 225.